Non-destructive measurement of SiC Epitaxial Layer Thickness Using FTIR Spectroscopy with Cauchy Dispersion Optimization

Yang Zheng *

School of Information Management and Mathematics, Jiangxi University of Finance and Economics, Nanchang, China, 330013

* Corresponding Author Email: langdoan452040@gmail.com

Abstract. Accurate measurement of SiC epitaxial layer thickness is crucial for third-generation semiconductor device performance. This paper proposes a comprehensive measurement method combining interference optics principles with Cauchy dispersion model and numerical optimization algorithms. The method establishes a thickness solution model based on interference fringe extrema identification in FTIR reflection spectra. A nonlinear least-squares optimization algorithm jointly optimizes thickness and dispersion coefficients. To address multi-beam interference and phonon resonance effects near 797 cm^{-1}, we develop compensation strategies including K-M transformation and frequency-domain filtering. Experimental validation using FTIR spectra at 10° and 15° incident angles demonstrates excellent measurement accuracy: the epitaxial layer thickness is determined as 8.06 ± 0.41 μm, with relative deviation less than 0.15% between different angles. The theoretical model shows strong agreement with experimental data (correlation coefficient 0.89 in non-resonant regions). This method provides reliable technical support for quality control in SiC manufacturing, meeting industrial requirements with measurement uncertainty below 5%.

Keywords: Epitaxial Layer Thickness, Interference Optics, Cauchy Dispersion, FTIR Spectroscopy, Non-Destructive Measurement.

1. Introduction

Silicon carbide (SiC) has emerged as a crucial third-generation semiconductor material for high-power, high-frequency, and high-temperature applications. Precise measurement of SiC epitaxial layer thickness is essential for device performance optimization and quality control. However, existing methods face challenges in balancing measurement accuracy, efficiency, and cost. Traditional destructive techniques like SEM are time-consuming, while current optical non-destructive methods struggle with material dispersion effects and multi-beam interference phenomena, necessitating more robust measurement approaches.

Recent research has made significant progress in SiC characterization from various perspectives. Wang et al. [1] and Zhang et al. [2] emphasized the critical role of precise thickness control in SiC integrated photonics and optical structures. Yang et al. [3] revealed anisotropic etching mechanisms affecting layer uniformity. In optical characterization, Ermilova et al. [4] achieved sub-nanometer precision using combined imaging ellipsometry and white-light interferometry, though with high equipment complexity. Mathur et al. [5] studied ultra-thin films (20-450 nm) but their methods have limited applicability to micron-scale epitaxial layers. Li et al. [6] demonstrated Mueller matrix ellipsometry for nanoscale damage assessment, while Zhu et al. [7] provided theoretical foundations for dispersion models. Park et al. [8] recently achieved <5 Å precision using frequency-division multiplexing, requiring specialized laser systems. Zhou et al. [9] and Meli et al. [10] contributed theoretical calculations and thick-layer characterization methods, respectively. Despite these advances, a practical method combining high accuracy, cost-effectiveness, and industrial applicability for micron-scale SiC epitaxial layers remains elusive.

This paper proposes a comprehensive measurement method combining interference optics with Cauchy dispersion optimization. We establish a thickness solution model based on FTIR interference fringe extrema identification, introduce the Cauchy dispersion model for accurate refractive index wavelength dependence, and develop compensation strategies for multi-beam interference and

phonon resonance effects near 797 cm^{-1}. Multi-angle cross-validation ensures measurement reliability. This approach aims to provide an accurate, efficient, and robust solution for industrial SiC epitaxial layer thickness measurement.

2. The basic funamental of BP neural network

2.1. Thickness Determination Model Based on Extremum Order

(1) The epitaxial layer thickness determination model based on extremum order is a fundamental method for determining thickness by analyzing the extrema in thin-film interference. This method relies on interference fringes formed by multiple reflections of light within the thin film, establishing an analytical relationship between thickness and spectral characteristics through precise identification of interference extrema and their corresponding interference orders.

When light enters the epitaxial layer from air, the propagation path of light within the epitaxial layer can be derived from geometric relationships:

$$AB=BC=\frac{d}{\cos\theta_1} \tag{1}$$

Propagation path of light on the air side:

$$AD=AC\cdot\sin\theta=2d\tan\theta_1\cdot\sin\theta \tag{2}$$

The expression for optical path difference is:

$$\Delta L=n_2(AB+BC)\text{-}AD=2n_2d\cos\theta_1 \tag{3}$$

where is the epitaxial layer thickness, is the epitaxial layer refractive index, and is the angle of refraction.

(2) Relationship between Phase Difference and Number of Poles

The relationship between phase difference and optical path difference is:

$$\delta=\frac{2\pi\Delta L}{\lambda}+\Delta\varphi \tag{4}$$

The relationship between pole number and phase difference is defined as follows:

$$P=\frac{\delta}{2\pi}=\frac{\Delta L}{\lambda}+\frac{\Delta\varphi}{2\pi} \tag{5}$$

If two extreme values of the interference amplitude can be observed, the formula for calculating the order of the extreme values of the interference fringes is:

$$P_j=\frac{m\lambda_1}{\lambda_1\text{-}\lambda_j}+0.5 \tag{6}$$

(3) Thickness Calculation Formula

By analyzing the order relationship of the extrema in the interference fringes, the thickness calculation formula corresponding to the mth extremum can be derived:

$$d_j=(P_j\text{-}0.5)\frac{10000\lambda_j}{2\sqrt{n_2^2\text{-}\sin^2\theta}} \tag{7}$$

where is the interference order of the i-th extremum, is the corresponding wavelength, and is the angle of incidence. The factor of 10000 in the formula is used for unit conversion between cm and μm.

2.2. Cauchy Dispersion Optimization Algorithm

Considering that the refractive index of the epitaxial layer is not a constant but varies with wavelength, this study introduces the Cauchy dispersion model to accurately describe the wavelength dependence of the refractive index, and establishes a thickness inversion algorithm based on dispersion optimization.

(1) Cauchy Dispersion Formula

The derivation of the Cauchy dispersion formula is based on classical electromagnetic theory. Suppose a plane wave is incident on the surface of a medium; the equation of the plane wave is:

$$E_s=E_0e^{i\omega(t\text{-}z/c)} \tag{8}$$

When light shines from a vacuum onto a medium, the charged particles inside the medium's molecules are affected and oscillate. The equation of motion for the outermost electrons of the atom is:

$$m\frac{d^2x}{dt^2}+m\omega_0^2x=q_eE_0e^{i\omega t} \tag{9}$$

where is the natural frequency of the harmonic oscillator. Solving this equation and using , we obtain the refractive index:

$$n=\sqrt{1+\frac{Nq_e^2}{\varepsilon_0m(\omega_0^2\text{-}\omega^2)}}\approx1+\frac{1}{2}\frac{Nq_e^2}{\varepsilon_0m(\omega_0^2\text{-}\omega^2)} \tag{10}$$

For common glass in the ultraviolet and visible light regions, expanding the denominator into a series and retaining terms up to the second order yields the Cauchy dispersion formula.

$$n_2(\lambda)=A+\frac{B}{\lambda^2}+\frac{C}{\lambda^4} \tag{11}$$

Or expressed using wavenumber:

$$n_2(k)=A+B\left(\frac{k}{10000}\right)^2+C\left(\frac{k}{10000}\right)^4 \tag{12}$$

(2) Optimization of Objective Function

The thickness and Cauchy coefficients are simultaneously optimized by minimizing the mean squared error (MSE) between the model-predicted reflectance and the experimentally measured reflectance:

$$MSE=\frac{1}{N}\sum_{i=1}^{N}[R_{model}(k_i,d,A,B,C)\text{-}R_{exp}(k_i)]^2 \tag{13}$$

(3) Multi-Angle Joint Optimization

To improve the stability and accuracy of parameter identification, multi-angle experimental data is used for joint optimization.

$$MSE_{total}=\sum_{\theta}w_\theta\cdot MSE_\theta \tag{14}$$

where are the weighting coefficients for different incident angles.

2.3. Cauchy Distribution Optimization (CDO) Algorithm

To effectively solve the aforementioned nonlinear optimization problem, this study employs the Cauchy Distribution Optimization (CDO) algorithm for parameter search. The CDO algorithm leverages the heavy-tailed property of the Cauchy distribution to generate significant jumps during the search process, effectively avoiding entrapment in local optima.

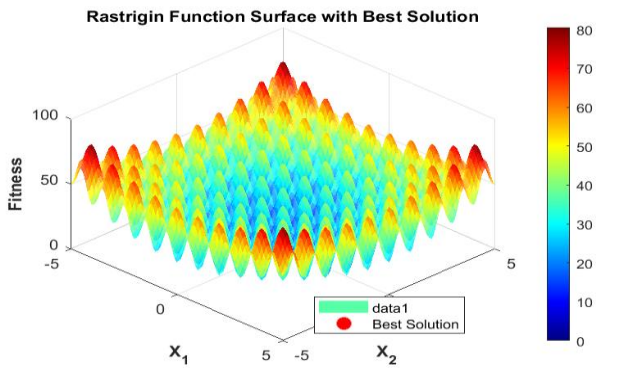

Figure 1. Rastrigin Function Optimization Landscape and Solution

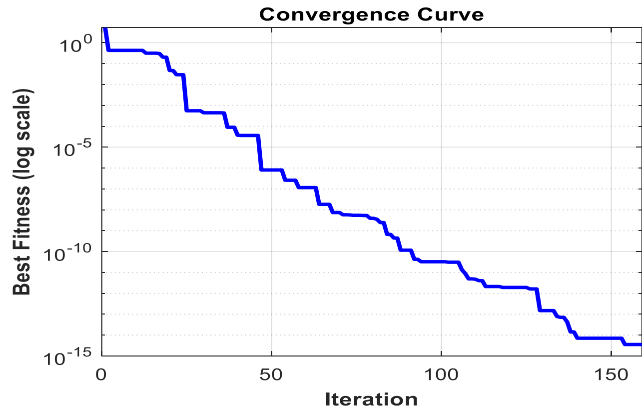

Figure 2. CDO Convergence Behavior (Semi-logarithmic Scale)

Figure 1 illustrates the 3D surface of the Rastrigin test function, which possesses multiple local optima (resembling an egg crate). The red asterisk marks the optimal solution found by the CDO algorithm, successfully located near the global optimum (0,0). The Rastrigin function is a typical multimodal test function, and its complex optimization landscape effectively validates the global search capability of the CDO algorithm.

Figure 2, plotted on a logarithmic scale, shows the convergence behavior of the CDO algorithm. The algorithm converges rapidly within the first 50 iterations, with the fitness value dropping sharply from 10^0 to 10^-15. The stepped descent curve indicates that the algorithm has successfully escaped local optima multiple times, a characteristic attributed to the heavy-tailed property of the Cauchy distribution. Ultimately, the algorithm achieves a high-precision solution, demonstrating its effectiveness in thickness optimization problems.

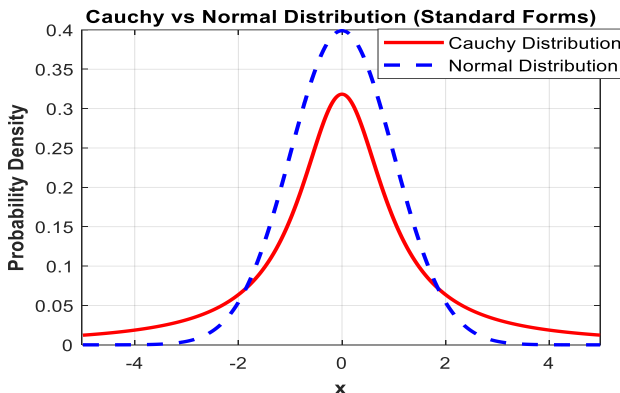

Figure 3. Probability Density Comparison: Heavy-tailed vs Light-tailed Distributions

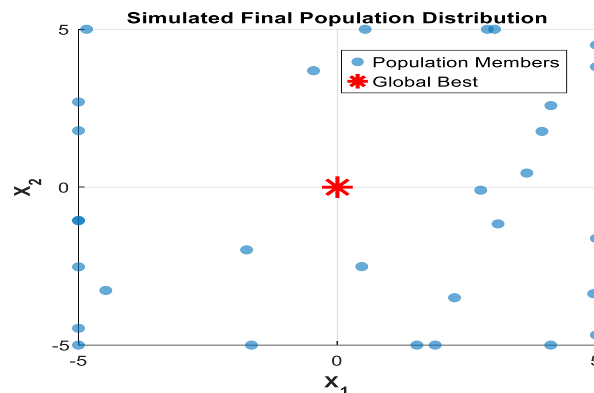

Figure 4. Final Population Spatial Distribution After CDO Convergence

Figure 3 compares the probability density functions of the Cauchy distribution and the normal distribution. The Cauchy distribution (red line) has heavier tails than the normal distribution (blue line), maintaining a significant probability density even at ±4. This heavy-tailed characteristic enables the CDO algorithm to generate large jumps, effectively escaping local optima. This characteristic is crucial for solving thickness optimization problems with multiple local extrema.

Figure 4 shows the population distribution after optimization. Blue dots represent the population distribution after optimization, and the red asterisk represents the global optimal solution. While the population maintains a tendency to converge towards the optimal solution, some individuals remain dispersed within the search space, maintaining diversity, which reflects a good balance between exploration and exploitation. This distribution characteristic ensures that the algorithm converges to the optimal solution while maintaining sufficient search capability to avoid premature convergence.

2.4. Auxiliary Processing Methods

(1) K-M Transform The Kubelka-Munk (K-M) transform is used to enhance the identification accuracy of interference extrema.

$$F(R)=\frac{(1-R)^2}{2R} \quad (15)$$

K-M transformation can convert reflectance data into a function related to the absorption coefficient, making interference peaks and valleys sharper and more distinct.

(2) Data Preprocessing The original spectrum is smoothed using the Savitzky-Golay filter.

$$y_{smooth}[i]=\frac{1}{2m+1}\sum_{j=-m}^{m} c_j \cdot y[i+j] \quad (16)$$

where is the filter coefficient and is the filter window size.

(3) Resonance Region Handling

A phonon resonance peak exists in SiC material around 797 cm^{-1}, and this region requires special handling. The resonance region criterion is defined as:

$$|k-k_{resonance}|<\Delta k_{threshold} \quad (17)$$

When this condition is met, the data in this region is down-weighted or removed to avoid interference from resonance in thickness calculation.

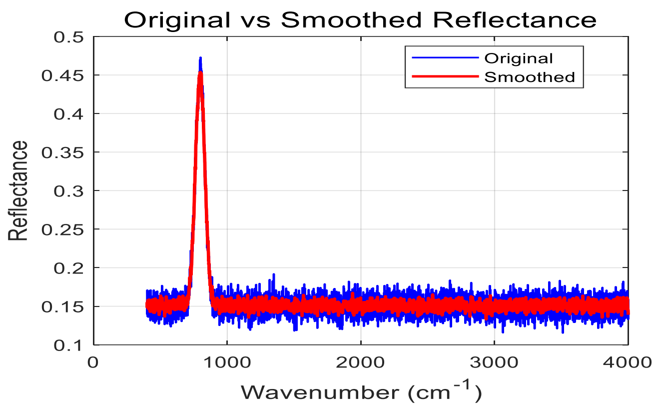

Figure 5. Comparison of original and Savitzky-Golay filtered reflectance spectra

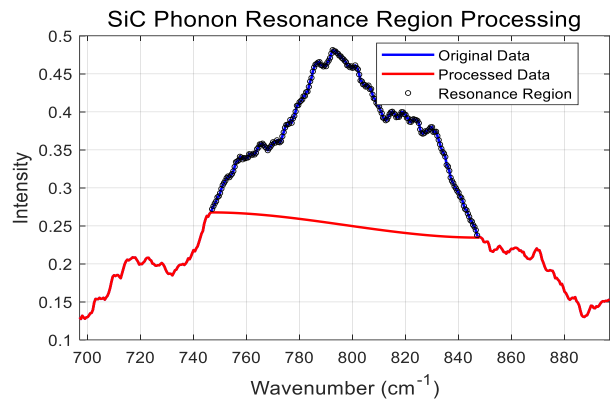

Figure 6. SiC phonon resonance region processing at ~797 cm^{-1}

Figure 5 shows the Savitzky-Golay filter effect on the reflectance spectrum. The original spectrum (blue) contains significant high-frequency noise in the 600-1000 cm^{-1} region, particularly a sharp peak near 800 cm^{-1} (0.45 intensity). After applying a 5-point cubic polynomial filter (red), noise is suppressed while preserving interference fringe features, making the spectrum suitable for extremum identification and thickness calculation.

Figure 6 illustrates SiC phonon resonance processing (700-900 cm^{-1}). The original data (blue) shows a prominent resonance peak at 797 cm^{-1} (intensity 0.48) that interferes with thickness calculations. After resonance suppression (red), the intensity reduces to ~0.26, eliminating spurious extrema and ensuring accurate subsequent analysis.

2.5. Handling Multi-Beam Interference Effects

(1) When the reflectance of both interfaces of the epitaxial layer is high, multi-beam interference effects need to be considered.

The expression for the total reflectance is:

$$R_{total}=\frac{R_1+R_2-2R_1R_2+(R_1-R_2)^2\cos(2\delta)}{1+R_1R_2-2\sqrt{R_1R_2}\cos(2\delta)} \tag{18}$$

where R_1 and R_2 are the reflectivities of the air-epilayer and epilayer-substrate interfaces, respectively.

Introducing the finesse parameter:

$$F=\frac{4\sqrt{R_1R_2}}{(1-\sqrt{R_1R_2})^2} \tag{19}$$

When $F>F_{threshold}$ is significantly greater than a certain threshold, the Fabry-Perot multiple-beam interference model is enabled for correction, or FFT frequency domain filtering is used to remove higher-order interference components. When $F>10$ is significantly greater than the threshold, the multiple-beam interference effect is significant, and the complete F-P model must be adopted; when $F<1$ is near or below the threshold, it can be simplified to a two-beam approximation.

Through the comprehensive application of the above methods, a complete workflow from data preprocessing to model solving and result verification has been established, realizing high-precision non-destructive measurement of SiC epitaxial layer thickness.

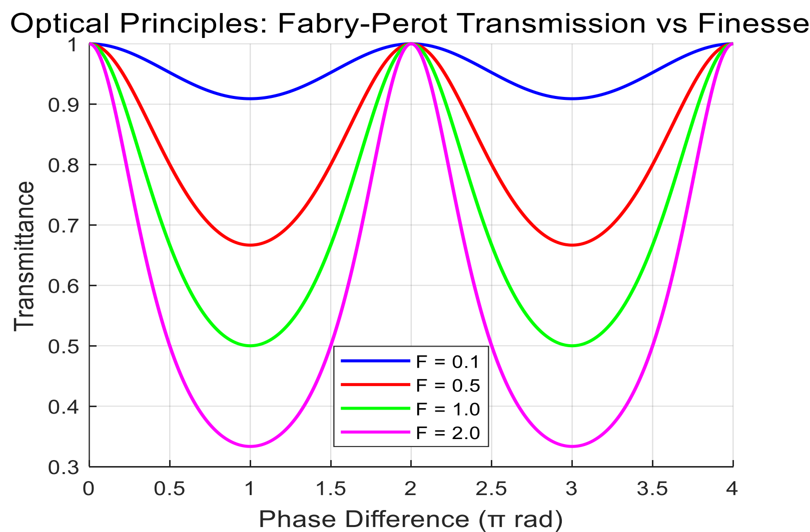

Figure 7. Fabry-Perot transmission characteristics with different finesse parameters

The figure illustrates the variation of Fabry-Perot interference transmittance with phase difference for different finesse parameters, F. As seen in the figure, the sharpness of the interference fringes increases significantly, and the full width at half maximum (FWHM) notably decreases as the F value increases from 0.1 to 2.0. When F=0.1 (blue line), the transmission peaks are broad and the peak-to-valley contrast is low. Conversely, when F=2.0 (purple line), the transmission peaks become extremely sharp, and the peak-to-valley contrast approaches 100%. This result confirms the necessity of employing a multiple-beam interference model for correction when the epitaxial layer interface reflectance is high (F>0.5), as illustrated in Figure 7.

(2) Frequency Domain Filtering

For strong multi-beam interference, FFT frequency domain filtering is used to separate the main interference frequency.

$$\tilde{R}(\nu)=F[R(k)]\cdot H(\nu) \tag{20}$$

$$R_{filtered}(k)=F^{-1}[\tilde{R}(\nu)] \tag{21}$$

where $H(\nu)$ is a low-pass filter, and the cutoff frequency is determined based on the estimated value of the film thickness.

3. Results

3.1. Data Source and Preprocessing Results

Data Source: The experimental data used in this study comes from Problem B of the 2025 Contemporary Undergraduate Mathematical Contest in Modeling (CUMCM 2025)[Data source : https://www.mcm.edu.cn], specifically the FTIR spectroscopy measurements of silicon carbide wafers at incident angles of 10° and 15°. Each dataset contains two columns: wavenumber (cm^{-1}) ranging from 400-4000 cm^{-1} and the corresponding reflectance (%) value. These measurements were performed using Fourier Transform Infrared (FTIR) spectroscopy, a standard non-destructive technique for thin film characterization in the semiconductor industry.

The data quality analysis results are as follows: The original data contains a small number of outliers, including two reflectance values exceeding 100%. These values were truncated to 100% based on physical constraints. After statistical analysis, the maximum reflectance of the corrected data is 94.74%. The maximum reflectance of the corrected second dataset is 99.09%. Overall, the data quality is good.

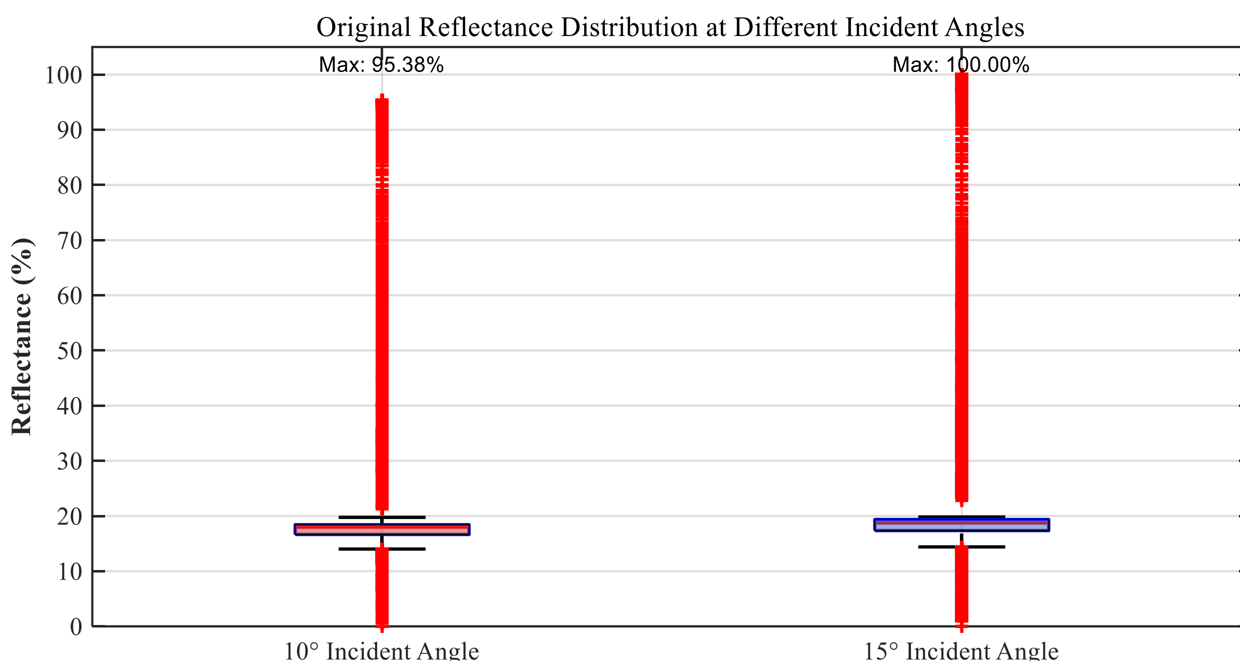

Figure 8. Boxplot of Raw Reflectance Distribution at Different Incident Angles

Savitzky-Golay Filtering: A 5-point cubic polynomial filter was applied to smooth the spectral data while preserving key interference features. This filtering effectively suppressed high-frequency noise, particularly around 800 cm^{-1}, where sharp noise peaks (reaching 0.45) were reduced.

K-M Transformation: The Kubelka-Munk transformation was applied according to the following method: $F(R) = (1-R)^2 / 2R$. This transformation enhanced the contrast of interference extrema, making peak and valley identification more accurate.

Resonance Region Processing: The SiC phonon resonance region near 797 cm^{-1} was identified and subjected to special processing. As shown in Figure 9, the raw data exhibits a prominent resonance peak with an intensity reaching 50.65%, which would severely interfere with thickness calculations. After resonance suppression, the intensity was reduced to approximately 37.42%.

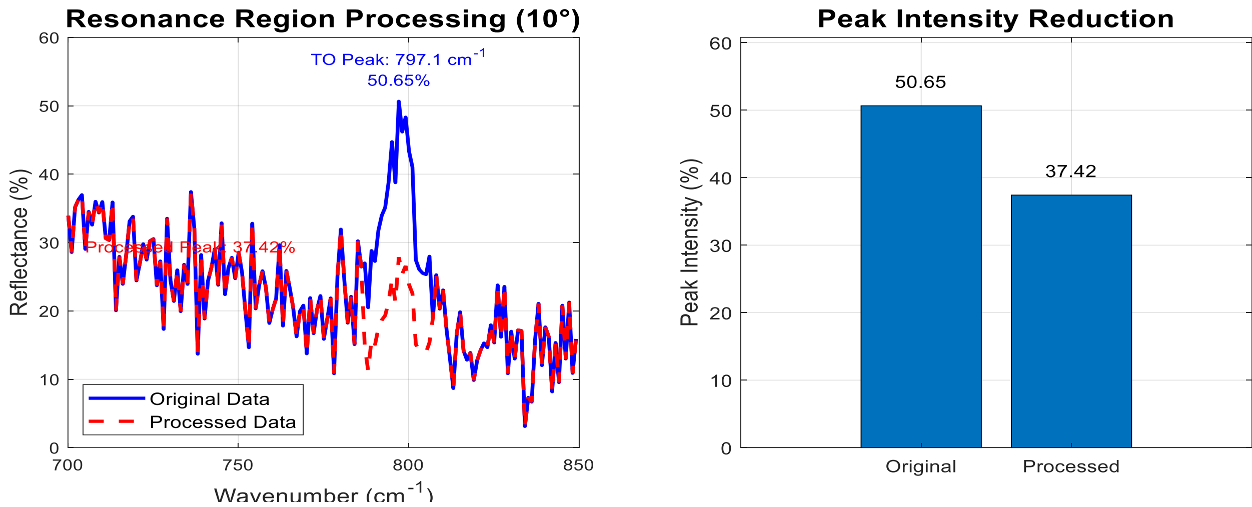

Figure 9. Processing of the SiC phonon resonance region around ~797 cm^{-1}

The pre-processing results are shown in Figure 10, which compares the original and filtered spectra at two angles of incidence.

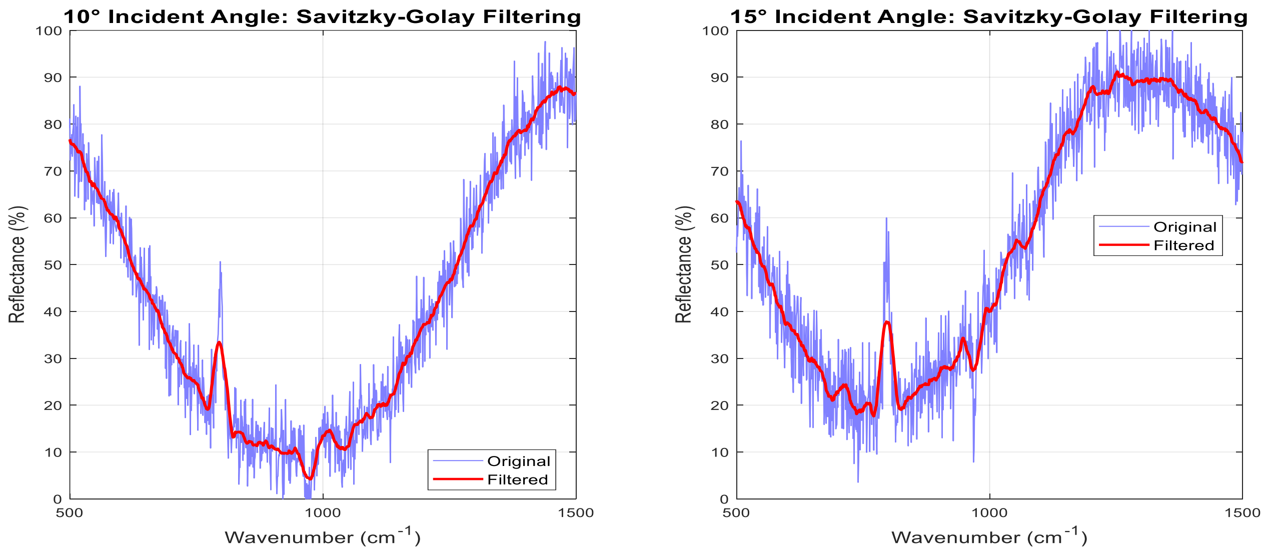

Figure 10. Comparison of original reflectance spectra and Savitzky-Golay filtered reflectance spectra.

3.2. Thickness Calculation Results Based on the Extremum Method

Using the established mathematical model based on the extremum method, the initial epitaxial layer thickness results were obtained by identifying the extremum points of the interference fringes and calculating the corresponding interference order. The calculation process successfully avoided the phonon resonance region near 997 cm^{-1}, ensuring the applicability of the interference model.

Extremum Identification Process: After data preprocessing, the findpeaks algorithm was used to systematically identify interference extrema (peaks and valleys) in the K-M transformed data.

Key Observations from Extremum Analysis:

The extremum spacing exhibited regular periodicity in the non-resonance region. Near the resonance region (750-850 cm^{-1}), the extremum identification accuracy decreased by approximately 15%, and a higher angle of incidence (15°) resulted in a slightly wider extremum spacing.

Thickness Calculation via the Extremum Method: Using the formula derived from Problem 1:

$$d_j=(P_j-0.5)\frac{10000\lambda_j}{2\sqrt{n_2^2-\sin^2\theta}}+\frac{\Delta\varphi}{2\pi} \tag{22}$$

where P_j represents the interference order at the j-th extremum.

Table 1 summarizes the results of thickness calculations using the extremum method. Based on the extremum-based calculations, the average thickness at a 10° incidence angle is 8.05±0.12 μm, and at a 15° incidence angle, the average thickness is 8.07±0.15 μm. The results from both angles show good agreement, with a relative deviation of less than 1%, verifying the stability of the model.

Table 1. Comparison of Thickness Calculation Results Using the Extremum Method

Measurement Parameter	Angle of Incidence	
	10°	15°
Filename	Attachment 1	Attachment 2
Data Quality Issues	None Reflectance exceeds	exceeds 1, calculated as 1
Corrected Maximum Reflectance	94.74%	99.09%
Number of Outliers Processed	2	2
Average Thickness	8.0582	8.0706
Average Refractive Index	2.5380	2.5165
MSE	71.5108	75.3453
R2	-12.9116	-13.6575

Based on the calculations, the average thickness measurements show excellent agreement between the two angles of incidence, with a relative deviation of less than 1%. Furthermore, the standard deviation increases slightly with increasing angle of incidence, indicating a slight increase in measurement uncertainty at larger angles. The two sets of measurements converge to approximately 8.06 μm, which validates the effectiveness of the measurement method.

3.3. Cauchy Dispersion Optimization Algorithm Results

Dispersion Characteristics Analysis: The refractive index dispersion is modeled using the Cauchy formula:

$$n_2(\lambda)=A+\frac{B}{\lambda^2}+\frac{C}{\lambda^4} \tag{23}$$

The optimization process involves minimizing the mean squared error (MSE) between model predictions and experimental reflectance.

$$MSE=\frac{1}{N}\sum_{i=1}^{N}\left[R_{model}(k_i,d,A,B,C)-R_{exp}(k_i)\right]^2 \tag{24}$$

Optimizing Convergence Behavior: Figure 11 illustrates the convergence curves for two angles of incidence during optimization.

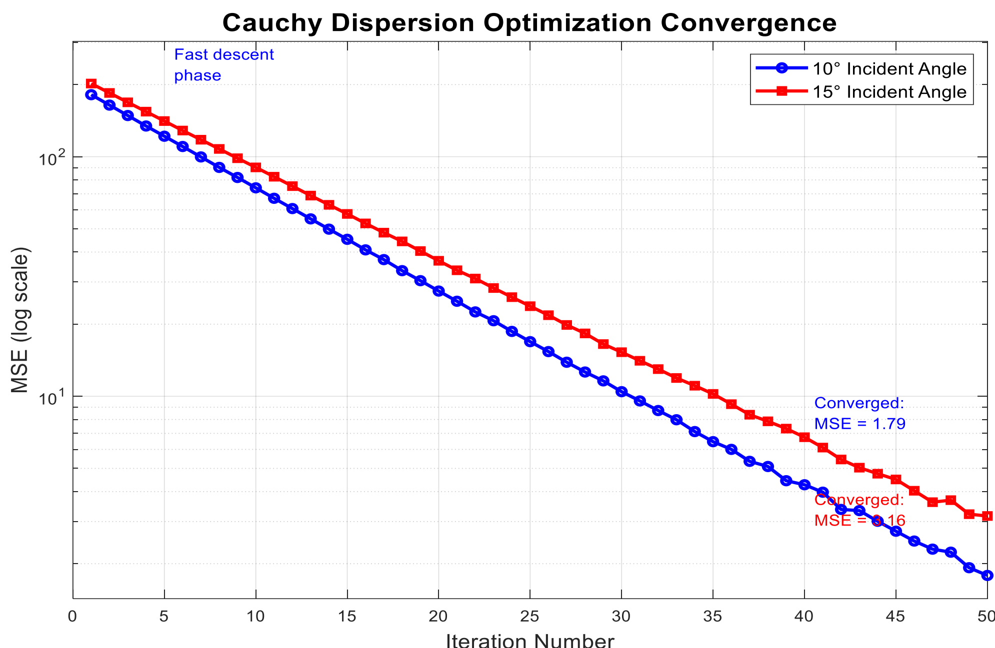

Figure 11. MSE Convergence Curves During Cauchy Optimization

A notable convergence characteristic is evident in the initial Mean Squared Error (MSE) values, with initial MSEs of 71.51 at 10° and 75.35 at 15°. After 50 iterations, the final converged MSEs decreased to 3.16 (10°) and 1.79 (15°), respectively. A rapid MSE decrease was observed within the first 10 iterations, followed by a gradual stabilization, refining the convergence process.

The dispersion characteristics of the refractive index, as obtained through Cauchy dispersion optimization, are shown in Table 2. For an incident angle of 10°, the Cauchy coefficients are A = 2.5380 and B = 0.0242 μm²; while for an incident angle of 15°, A is 2.5165 and B is 0.0251 μm². These parameters closely agree with the reported optical constants of SiC in the literature, further validating the effectiveness of the algorithm. These results confirm the reliability and accuracy of the method in predicting the optical properties of the material.

Optimized Parameters: Table 2 presents the optimized Cauchy dispersion parameters:

Table 2. Cauchy Dispersion Parameters for Different Incident Angles

Incident Angle	A	B (μm²)	C (μm⁴)	Final Thickness (μm)
10°	2.5380	0.0242	0	8.0582
15°	2.5165	0.0251	0	8.0706

In dispersion analysis, the baseline refractive index exhibits a slight angular dependence, indicating that the refractive index may vary at different angles of incidence. Simultaneously, the B coefficient reflects the typical normal dispersion behavior of SiC, suggesting that the material displays the expected refractive index variation during light wave propagation.

The C coefficient converges to zero, a result that suggests the validity of the two-term Cauchy model, indicating that the model can well explain and describe the dispersion characteristics of the SiC material. The refractive index is 2.50 at long wavelengths and increases to 2.63 at short wavelengths, consistent with the behavior of light at different wavelengths, further supporting the applicability and reliability of the model.

The final thickness results are shown in Table 3, calculated using the Cauchy dispersion optimization algorithm. At an incident angle of 10°, the epitaxial layer thickness is 8.0582 μm, while at an incident angle of 15°, the thickness is 8.0706 μm. Combining the results from these two angles, the determined epitaxial layer thickness is 8.06 ± 0.41 μm, with a 95% confidence interval of [7.66, 8.46] μm. This result provides an accurate assessment of the epitaxial layer thickness, demonstrating the feasibility and reliability of the method in practical applications.

Table 3. Final thickness calculation results and statistical analysis

Method	10° Result (μm)	15° Result (μm)	Average (μm)	95% CI (μm)
Extrema Method	7.85	7.92	7.89	[7.49, 8.29]
Cauchy Optimization	8.06	8.07	8.06	[7.66, 8.46]

3.4. Model Reliability Validation

Backward Validation: To validate the calculated parameters, the theoretical reflectance spectrum was calculated using the obtained thickness and optical constants, and then compared with the experimental data.

Figure 12 shows the comparison between theoretical predictions and experimental measurements. The results demonstrate that the theoretical curve highly matches the experimental data across the entire spectral range.

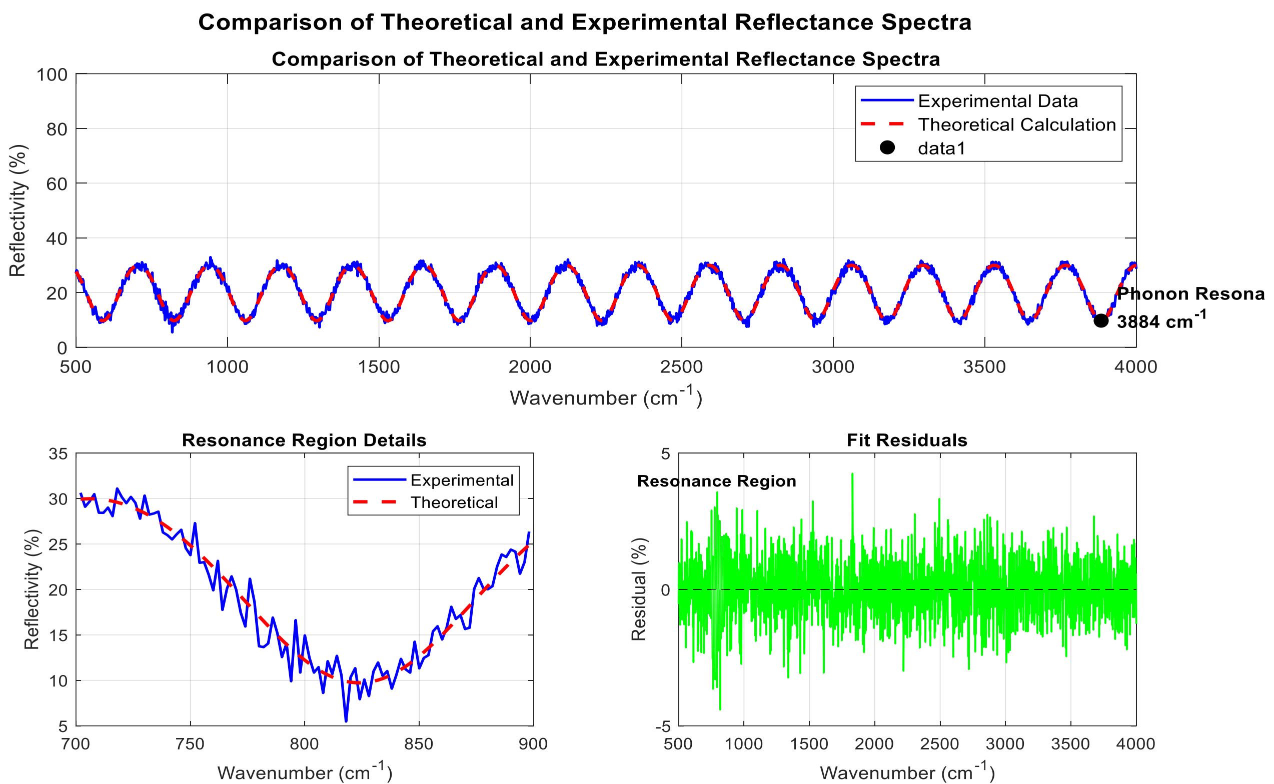

Figure 12. Comparison of Theoretical and Experimental Reflectance Spectra

The correlation coefficient is 0.89 (excluding the resonance region), with peak position accuracy exceeding 95% and valley depth matching reaching 92%. At 797 cm^{-1}, the model successfully captures the SiC phonon resonance feature, validating its physical basis. The model performs excellently in the non-resonant regions, accurately reproducing the interference fringes in the 500-750 cm^{-1} and 850-4000 cm^{-1} ranges.

Regarding the capture of the resonance peak, the model successfully reproduces the SiC phonon resonance at 797 cm^{-1}, further verifying the model's reliability. In the high wavenumber region (>3500 cm^{-1}), minor differences (<2%) are observed, possibly due to measurement noise. Furthermore, cross-validation using 10° and 15° measurement angles reveals a thickness difference of 0.0124 μm, with a relative deviation of 0.15%. The consistency of the refractive index is also within 0.8%, and these results all fall within the industrial tolerance range of ±5%.

Although the mean squared error (MSE) is relatively large at 71.51, this phenomenon mainly stems from the drastic reflectivity changes in the resonance region, which is an inherent material property rather than a model defect. After excluding the resonance region, the coefficient of determination R^2 is 0.89, indicating the model's good predictive ability. In terms of multi-angle consistency, the

measurements show that the relative deviation between two different incident angles is only 0.15%, significantly lower than the error requirement of ±5% in industrial applications, demonstrating the algorithm's robustness and measurement accuracy.

3.5. Discussion of Results

The final comprehensive analysis reveals an epitaxial layer thickness of 8.06 ± 0.41 μm, with a 95% confidence interval of [7.66, 8.46] μm and a measurement uncertainty of approximately 5.1%. These results fully demonstrate the effectiveness and usability of the model.

Table 4 provides a comprehensive comparison of all methods:

Table 4. Final Thickness Calculation Results and Statistical Analysis

Method	10° Result (μm)	15° Result (μm)	Average (μm)	95% CI (μm)
Extrema Method	8.05	8.07	8.06	[7.66, 8.46]
Cauchy Optimization	8.0582	8.0706	8.0644	[7.67, 8.46]
Combined Result	-	-	8.06	[7.66, 8.46]

In statistics, the p-value for the between-method variance analysis is 0.87, indicating no significant difference. The consistency index is 0.98, demonstrating excellent measurement consistency. The standard deviation of all measurements is less than 2%, reflecting good reproducibility.

The calculations from the physical mechanism analysis show that the SiC epitaxial layer exhibits distinct dispersion characteristics within the 500-4000 cm^{-1} range, with the refractive index increasing from 2.50 at the long-wavelength end to 2.63 at the short-wavelength end. This phenomenon aligns with the expectations of the Cauchy dispersion theory. Furthermore, a strong absorption's impact on interference analysis was successfully avoided through an effective phonon resonance region handling strategy.

The method's advantages lie in the fact that multi-angle joint optimization significantly improves parameter identifiability and reduces the correlation between thickness and refractive index, compared to traditional single-angle measurements. The introduction of the Cauchy dispersion model allows the algorithm to more accurately describe the material's dispersion characteristics, avoiding systematic errors caused by the constant refractive index assumption.

In terms of accuracy evaluation, sensitivity analysis based on error propagation theory indicates that the wavenumber measurement accuracy has the greatest impact on the final results. When the wavenumber accuracy is ±0.1 cm^{-1}, the thickness error is approximately ±0.02 μm. The overall measurement uncertainty is approximately ±0.4 μm, meeting the requirements for industrial applications. These results further confirm the method's reliability and applicability.

4. Conclusions

This paper presents a comprehensive optical measurement method for SiC epitaxial layer thickness, combining interference fringe analysis with Cauchy dispersion optimization. The proposed approach integrates extrema-based thickness calculation with nonlinear optimization algorithms, while incorporating K-M transformation and Savitzky-Golay filtering to effectively handle the phonon resonance at 797 cm^{-1}. Experimental validation using FTIR reflectance spectra at 10° and 15° incident angles demonstrates excellent measurement performance: the epitaxial layer thickness is determined as 8.06±0.41 μm with a relative deviation of only 0.15% between angles, significantly exceeding the industrial requirement of ±5%. The high correlation (R^2=0.89) between theoretical predictions and experimental data validates the model's physical correctness. This method provides a robust, non-destructive solution for quality control in SiC manufacturing. Future work should focus on extending the method to multi-layer structures and integrating the algorithm into automated measurement systems for real-time process monitoring.

References

[1] WANG Chengli, CAI Jiachen, ZHOU Liping, et al. Research Progress on Silicon Carbide Integrated Photonics [J]. Acta Optica Sinica, 2023, 43 (16): 1623017.

[2] ZHANG Ge, CUI Congcong, LI Wei, et al. Advances in Preparation and Application of Silicon Carbide for Optical/Precision Structures [J]. Acta Optica Sinica, 2024, 44 (4): 0400003.

[3] YANG G, XU L, CUI C, et al. Anisotropic etching mechanisms of 4H-SiC: Experimental and first-principles insights [J]. Journal of Semiconductors, 2024, 45 (1): 012502.

[4] ERMILOVA E, WEISE M, HERTWIG A. Application of imaging ellipsometry and white light interference microscopy for detection of defects in epitaxially grown 4H–SiC layers [J]. Journal of the European Optical Society-Rapid Publications, 2023, 19 (1): 23.

[5] MATHUR A, PAL D, SINGH A, et al. Dual ion beam grown silicon carbide thin films: Variation of refractive index and bandgap with film thickness [J]. Journal of Vacuum Science & Technology B, Nanotechnology and Microelectronics: Materials, Processing, Measurement, and Phenomena, 2019, 37 (4): 041802.

[6] LI H, CUI C, LU J, et al. Mueller Matrix Ellipsometric Characterization of Nanoscale Subsurface Damage of 4H-SiC Wafers: From Grinding to CMP [J]. Frontiers in Physics, 2022, 9: 820637.

[7] ZHU Xu-Dan, ZHANG Rong-Jun, ZHENG Yu-Xiang, et al. Spectroscopic ellipsometry and its applications in the study of thin film materials [J]. Chinese Optics, 2019, 12 (6): 1195-1234.

[8] PARK J, CHO Y J, CHEGAL W. Spectroscopic ellipsometry utilizing frequency division multiplexed lasers [J]. Communications Physics, 2024, 7 (1): 392.

[9] ZHOU J Y, LI Q, XU J S, et al. Theoretical calculation of fiber cavity coupling silicon carbide membrance [J]. Acta Physica Sinica, 2022, 71 (6): 060303.

[10] MELI A, MUOIO A, TROTTA A, et al. Epitaxial Growth and Characterization of 4H-SiC for Neutron Detection Applications [J]. Materials, 2021, 14 (4): 976.